Nanoscale

Accepted Manuscript

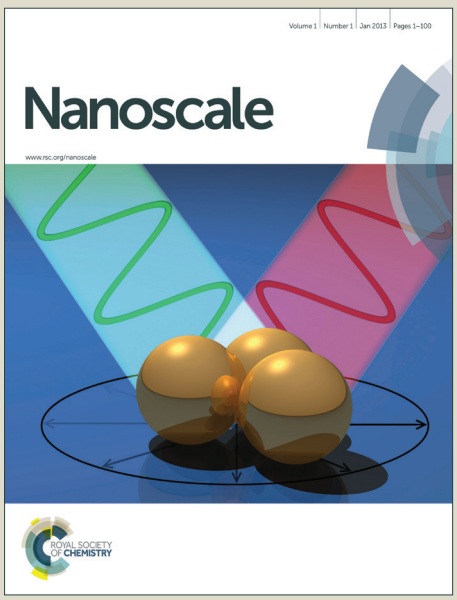

ROYAL SOCIETY OF CHEMISTRY

www.rsc.org/nanoscale

Cite this: DOI: 10.1039/c0xx00000x

www.rsc.org/xxxxxx

ARTICLE TYPE

Responsive polymer-fluorescent carbon nanoparticle hybrid nanogels for optical temperature sensing, near-infrared light-responsive drug release, and tumor cell imaging

Hui Wang,[a] Fuyou Ke,[a] Anton Mararenko,[a] Zengyan Wei,[b] Probal Banerjee[a] and Shuiqin Zhou[a*]

Received (in XXX, XXX) Xth XXXXXXXXX 20XX, Accepted Xth XXXXXXXXX 20XX
DOI: 10.1039/b000000x

Fluorescent carbon nanoparticles (FCNPs) have been successfully immobilized into the poly(N-isopropylacrylamide-co-acrylamide) [poly(NIPAM-AAm)] nanogels based on a one-pot precipitation copolymerization of NIPAM monomers with the hydrogen bonded FCNP-AAm complex monomers in water. The resultant poly(NIPAM-AAm)-FCNP hybrid nanogels can combine functions from each building block for fluorescent temperature sensing, cell imaging, and near-infrared (NIR) light responsive drug delivery. The FCNPs in the hybrid nanogels not only emit bright and stable photoluminescence (PL) and exhibit up-conversion PL property, but also increase the loading capacity of the nanogels for curcumin drug molecules. The reversible thermo-responsive swelling/shrinking transition of the poly(NIPAM-AAm) nanogel cannot only modify the physicochemical environment of the FCNPs to manipulate the PL intensity for sensing the environmental temperature change, but also regulate the releasing rate of the loaded anticancer drug. In addition, the FCNPs embedded in the nanogels can convert the NIR light to heat, thus an exogenous NIR irradiation can further accelerate the drug release and enhance the therapeutic efficacy. The hybrid nanogels can overcome cellular barriers to enter the intracellular region and light up the mouse melanoma B16F10 cells upon a laser excitation. The demonstrated hybrid nanogels with nontoxic and optically active FCNPs immobilized in responsive polymer nanogels provide a promise to develop a new generation of multifunctional materials for biomedical applications.

1. Introduction

Multifunctional hybrid nanogels combining several useful properties in a single nanostructure have gained significant momentum because of their potential broad applications including as drug carriers, sensors, and bioimaging labels.[1-3] Polymer nanogels cannot only provide high drug loading capacity due to their porous structures and large surface areas, but also possess good biocompatibility due to their high water content and soft nature similar to natural extracellular matrices.[4,5] Recently, significant progress has been made to develop stimuli-responsive nanogels that can effectively regulate the release of the loaded drug molecules in response to a given stimulus such as a change in pH, temperature, redox activation, enzymatic activity, competitive binding, bacteria and glucose level.[6-12] However, these stimuli-responsive drug release strategies relying on the changes in specific physical or chemical properties of the environmental medium are sometimes limited for in vivo applications, because a harsh environmental change can cause severe side-effects to normal cells and tissues.[13] Light is a great candidate as an external stimulus to remotely control the drug release at a desired site and time, which is considered crucial to boosting drug efficacy in cancer treatment while minimizing side effects.[14] NIR light with low energy absorption and deep penetration for human tissue is a desirable choice and has been widely used as an external stimulus for photo-responsive drug carriers.[15-19] Based on the photothermal conversion ability of noble metal nanoparticles (NPs) under NIR irradiation, various kinds of noble metal NPs in specific size and shape have been used to synthesize multifunctional hybrid nanogels for light-controlled drug release.[20-24] Meanwhile, the noble metal component can also serve as an optical marker for tumor cell imaging.[25–27] However, several disadvantages are associated with the noble metal NPs for their use in biomedical areas, including the toxicity for neuronal cells, potential induction of oxidative stress processes in the body, and high cost.[28,29]

Fluorescent carbon nanoparticles (FCNPs), a kind of small carbon semiconductor quantum dots, have recently attracted great attention from an increasing number of researchers because of their excellent properties and potential wide applications.[30-33] Compared with noble metal NPs, FCNPs demonstrate lower toxicity and better biocompatibility according to their cytotoxic and in vivo toxic evaluation results.[34,35] In addition, the as-synthesized FCNPs with hydrophilic groups on their surface can directly disperse into aqueous media very well with no need for further surface modification.[36,37] More importantly, these FCNPs not only exhibit bright nonblinking PL with excellent photostability, but also have excellent photothermal conversion ability under NIR radiation.[38,39] So far, FCNPs have successfully demonstrated to be a promising candidate for applications as an optical code for biosensing and bioimaging and as a NIR photothermal therapeutic agent for treatment of solid tumors.[38-44]

Considering the unique materials properties of FCNPs and the advantages of the responsive polymer nanogels as drug carriers, it will be desirable to develop a new type of nanosystems that can combine the functions from both FCNPs and responsive nanogels. We expect that such a hybrid nanogel system comprised of both FCNPs and responsive nanogels cannot only maintain high drug loading capacity with controllable drug release profiles, but also serve as an optical code for bioimaging and biosensing.

The purpose of this manuscript is to develop a synthetic strategy to prepare a class of new hybrid nanogels from FCNPs and responsive polymers for multifunctional applications. Herein, we select the most widely studied polyNIPAM as a model responsive nanogel system so that a simple one-pot precipitation polymerization method in water can be applied. In order to effectively immobilize the FCNPs into the polymer nanogels, we select AAm as a comonomer to complex with the FCNPs via hydrogen bonding interactions with the surface hydroxyl/carboxyl groups on FCNPs. After copolymerization and crosslinking, we expect that the FCNPs will be randomly embedded in the resultant poly(NIPAM-AAm) nanogel networks, as illustrated in Fig. 1. In such a design, the FCNPs can serve as optically active component for fluorescent sensing, cellular imaging, and NIR photothermal conversion. The porous thermo-responsive poly(NIPAM-AAm) nanogel can serve as intelligent drug carriers with high drug loading capacity. In this work, a natural medicine of curcumin has been selected as a model anti-cancer drug to evaluate the drug carrier function of the hybrid nanogels. The embedded FCNPs should further enhance the curcumin loading capacity based on the hydrophobic associations between the conjugated carbon matrix in FCNPS and the curcumin molecules. The reversible swelling and shrinking of the nanogel in response to temperature change will not only modify the physicochemical environment of the embedded FCNPs to manipulate their optical properties for sensing the local temperature change, but also change the mesh size of the gel networks to regulate the drug release rate. Therefore, the resultant poly(NIPAM-AAm)-FCNP hybrid nanogels provide a multifunctional nanoplatform for simultaneous temperature sensing, cellular imaging, and intelligent dose of drug molecules under both endogeneous thermo-activation and exogenous NIR irradiation activation.

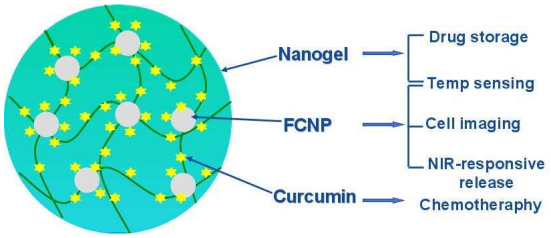

Fig. 1. Schematic illustration of multifunctional hybrid nanogels with the FCNPs randomly embedded in the thermo-responsive poly(NIPAM-AAm) gel network for integration of temperature sensing, cell imaging, and thermo-/NIR-responsive curcumin drug release.

2. Materials and methods

2.1 Materials

D(t)-Glucose was purchased from ACROS, and all other chemicals were purchased from Aldrich. NIPAM was recrystallized from a 1:1 hexane-acetone mixture and dried in vacuum. Curcumin was purified with anhydrous ethanol. Ammonium persulfate (APS), sodium dodecyl sulfate (SDS), N,N-methylenebisacrylamide (BIS), acrylamide (AAm), HCl (37%) were used as received without further purification. The water used in all experiments was of Millipore Milli-Q grade.

2.2. Synthesis of fluorescent carbon nanoparticles

FCNPs were synthesized via a one-step process based on a modified previously reported method.[45] In a typical synthesis, glucose (0.90 g) was dissolved in deionized water (10 mL). After intense sonication for 20 min, 10.0 mL of HCl (37 wt.%) was slowly added into the above solution. The mixed solution was then treated ultrasonically for 5 h and transferred into a 50 mL Teflon-lined stainless autoclave. The precursor solution was heated to and maintained at 120 °C. After 24 h, the solution was cooled naturally to room temperature. The resulted FCNPs were purified with repeated centrifugation and redispersion in water for three cycles. Finally, the aqueous dispersion of FCNPs were dialyzed for 7 days (Spectra/Por®molecularporous membrane tubing, cutoff 12,000-14,000) at room temperature (~22 °C). The aqueous dispersion of FCNPS was then collected and dried to get solid FCNPs.

2.3. Synthesis of FCNP-polymer hybrid nanogels

The multifunctional hybrid nanogels were prepared by one-pot free radical precipitation copolymerization of NIPAM and AAm in the aqueous dispersion of FCNPs using APS as an initiator. In a 250 mL round-bottom flask equipped with a stirrer, a N_2 gas inlet, and a condenser, 47.5 mL aqueous solution of FCNPs (0.1 g/L) was heated to 30 ° C, followed by addition of monomers of NIPAM (0.7024 g) and AAm (0.0509 g), crosslinker of BIS (0.0368 g), and surfactant of SDS (0.0254 g) under stirring. After the temperature was raised to 70 °C and maintained for 60 min under N_2 purge, the polymerization was initiated by adding 2.50 mL APS solution of 2 mM. The polymerization was allowed to proceed for 4 h. The solution was centrifuged three times at 20,000 rpm (30 min, Thermo Electron Co. SORVALL®RC-6 PLUS superspeed centrifuge) with the supernatant discarded and the precipitate redispersed in 50 mL deionized water. The resultant hybrid nanogels with a volume of 50 mL was further purified to remove the possibly unreacted monomers and free FCNPs by 3 days of dialysis (Spectra/Por®molecularporous membrane tubing, cutoff 12000-14000) against very frequently changed water at room temperature.

2.4. Preparation of curcumin-loaded hybrid nanogels

Curcumin, a kind of anti-cancer drug, was loaded into the hybrid nanogels by complexation method. The hybrid nanogel dispersion (5 mL, pH=4.0) placed in a vial was stirred in an ice water bath for 30 min. Then, 4 mL fresh curcumin solution of 1 mg/mL in anhydrous ethanol was added dropwisely into hybrid nanogel. The immediate slight cloudy revealed the complexation of the curcumin molecules with the hybrid nanogels. After stirring for 16 h under a dark light, the suspension was centrifuged at 5000 rpm for 30 min at 20 °C. The precipitate was washed with anhydrous ethanol to remove the unloaded curcumin and then redispersed in 5 mL HCl solution of pH=4.0. The curcumin-loaded hybrid nanogels were further purified by repeated centrifugation and washing until the supernatant is clear. All the washed solution and supernatant were collected and then diluted to 100 mL in water. The concentration of free curcumin was determined by UV-vis spectrometry at 421 nm. The drug loading content were calculated by $(M_0\text{-}M_t)/M_N\times100\%$, where M_0 and M_t are the mass of curcumin in the initial solution and the washed solution plus supernatant, respectively. M_N is the mass of nanogel used in the loading process.

2.5. Curcumin release from the hybrid nanogels

The in vitro release of curcumin from the hybrid nanogels was evaluated by the dialysis method. The purified curcumin-loaded

hybrid nanogels were redispersed in 10 mL very dilute HCl solution of pH=4.0. A dialysis bag filled with 1 mL such curcumin-loaded hybrid nanogel dispersion was immersed in 50 mL 0.005 M buffer solutions of pH = 6.10 but at different temperatures of 41, 39, 37, and 22 ^{o}C, respectively. The release experiments at physiological temperature of 37 ^{o}C were also performed with 5 min NIR (1.5 W/cm^2) irradiation at a certain time interval. The released curcumin outside of the dialysis bag was sampled at defined time period and assayed by UV-vis spectrometry at 421 nm. Cumulative release is expressed as the total percentage of drug released through the dialysis membrane over time.

2.6. Internalization of hybrid nanogels into mouse melanoma cells B16F10

Round glass cover slips were placed in wells of a 24-well plate and treated with 0.1% poly-L-lysine in 100 mM phosphate buffered saline (PBS) for 40 min. Following the treatment, the solution was aspirated and the wells were washed with PBS 3 times each. Next, B16F10 cells (2×10^4 cell/well) were plated on the glass coverslips at 80% confluence in DMEM containing 10% FBS and 1% penicillin-streptomycin. After 24 h, 500 μL of multifunctional hybrid nanogel (50 μg/mL) in serum-free DMEM were respectively added to the marked wells. In a control well, 500 μL of serum-free DMEM was added. The plate was incubated at 37 °C for 2 h. The medium was then aspirated and fresh serum-free DMEM was added to each well. Finally, the coverslips with cells were removed from the wells and mounted onto slides for confocal microscopy study.

2.7. In vitro cytotoxicity of hybrid nanogels and curcumin-loaded hybrid nanogels with or without NIR irradiation.

In this study, B16F10 cells were cultured in the 96 wells microplate in 100 μL medium containing about 2,000 cells seeded into each wells. After an overnight incubation for attaching, the medium was removed and another 100 μL medium containing different amount of hybrid nanogels or curcumin-loaded hybrid nanogels was added to make the final exact concentration of 200, 150, 100, and 50 μg/mL, respectively. Wells used the normal medium without drugs were used as control. For photothermal treatments, the cells in the wells were irradiated with 1.5 W/cm^2 NIR light for 5 min. After incubated for 24 h, 10 μL of 3-(4,5-dimethyl-2-thiazolyl)-2,5-diphenyltetrazolium bromide (MTT) solution (5 mg/ml in PBS) was added into the wells. The wells were further incubated in a humidified environment of 5 % CO_2 and 37 °C for 2 h. The medium were removed after 2 h and 100 μL of DMSO solution was added. The plates were gently agitated until the formazan precipitate was dissolved, followed by measurement of OD value by spectrophotometer at 570 nm and 690 nm.

2.8. Characterization

The UV-vis absorption spectra were obtained on a Thermo Electron Co. Helios β UV-vis Spectrometer. The FT-IR spectra were recorded with a Nicolet Instrument Co. MAGNA-IR 750 Fourier transform infrared spectrometer. The PL spectra were respectively obtained on a JOBIN YVON Co. FluoroMax®-3 Spectrofluorometer equipped with a Hamamatsu R928P photomultiplier tube, calibrated photodiode for excitation reference correction from 200 to 980 nm, and an integration time of 1 s. The transmission electron microscopy (TEM) images were taken on a FEI TECNAI transmission electron microscope at an accelerating voltage of 100 kV. High-resolution transmission electron microscopy images were characterized by JEM 2100 with an acceleration voltage of 200 kV. The B16F10 cells incorporated with hybrid NPs were imaged using a confocal laser scanning microscopy (LEICA TCS SP2 AOBS^{TM}) equipped with a HC PL APO CS 20×0.7 DRY len. A UV (405 nm) light was used as the light source. The corresponding image detection channel wavelength ranges are 480–560 nm. Dynamic light scattering (DLS) was performed on a standard laser light scattering spectrometer (BI-200SM) equipped with a BI-9000 AT digital time correlator (Brookhaven Instruments, Inc.) to measure the hydrodynamic radius (R_h) distributions. A He-Ne laser (35 mW, 633 nm) was used as the light source. The hybrid nanogel dispersion was passed through Millipore Millex-HV filters with a pore size of 0.45 μm to remove dust before the DLS measurement.

3. Results and Discussion

3.1. Synthesis, structure, and properties of poly(NIPAM-AAm)-FCNP hybrid nanogels

Our strategy to prepare the thermo-responsive poly(NIPAM-AAm)-FCNP hybrid nanogel with FCNPs as optical marker involves the first synthesis of water-dispersible FCNPs bearing surface carboxyl/hydroxyl groups, followed by precipitation copolymerization of the NIPAM and AAm comonomers that are complexed with FCNPs. The FCNPs have been successfully synthesized via a one-pot acid assisted hydrothermal decomposition of glucose. Fig. 2a shows the typical TEM image of the obtained FCNPs, which shows a spherical morphology with an average size of ~13 nm in diameter. The DLS study result (Figure S1 in Supporting information) demonstrates that the FCNPs have a narrow size distribution with an average hydrodynamic diameter (D_h) of 18 nm in distilled water. The FCNPs do not form aggregates, indicating a good stability in water. The slightly larger diameter of FCNPs in water than in dried state is understandable, because the hydrophilic carboxyl/hydroxyl groups on the surface of the FCNPs form an extra hydrated layer in water. As shown in Fig. 3b, the FT-IR spectrum of the FCNPs shows an apparent broad absorption peak of hydroxyl (-OH) groups at about 3360 cm^{-1} and a characteristic absorption peak at 1705 cm^{-1}of carboxylic acid (-COOH) group conjugated with condensed aromatic carbons. These hydrophilic –COOH and/or –OH groups on the FCNPs not only enable the FCNPs to be dispersed very well in water,[36,37] but also can form hydrogen bonds with the amide groups in the AAm monomers, thus forming FCNP-AAm complexes in water. After the copolymerization and crosslinking of these FCNP-complexed AAm monomers with the NIPAM monomers, it is expected that the FCNPs will be immobilized into the resultant thermo-responsive poly(NIPAM-AAm) nanogel network. Fig. 2b shows a typical TEM image of the resultant poly(NIPAM-AAm)-FCNP hybrid nanogel particles in dried state. The dried hybrid nanogels have a spherical shape with an average diameter about 180 nm. It can be seen that some FCNPs are randomly encapsulated in the poly(NIPAM-AAm) nanogel, although the contrast of FCNPs with the dried nanogel is weak. Fig. 2c shows the sectional high-resolution TEM image of a typical FCNP embedded in the hybrid nanogel. Some nanocrystals with a size about 4 nm can be easily found in the FCNPs, which manifest that the FCNPs are composed of many crystallized fluorescent carbon dots randomly distributed in the amorphous carbon. The 2D lattice fringes of the small nanocrystals demonstrate an interplanar distance about 0.315 nm, which corresponds to the <002> lattice planes of graphitic (sp^2) carbon.

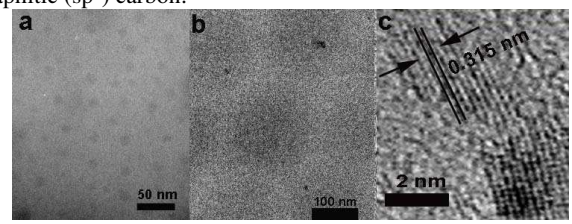

Fig. 2. (a) TEM image of the as-obtained FCNPs; (b) TEM image of the poly(NIPAM-AAm)-FCNP hybrid nanogels; (c) sectional HRTEM image of a typical FCNP embedded in hybrid nanogel.

Fig. 3a shows typical UV–visible absorption spectra of the FCNPs, poly(NIPAM-AAm) nanogels, and poly(NIPAM-AAm)-FCNP hybrid nanogels, respectively. While the poly(NIPAM-AAm) nangoel has no significant absorption at wavelength above 280 nm, there is a clear broad peak centered at 280 nm in the curve of FCNPs, which represent the typical absorption of an aromatic π system and is similar to that of polycyclic aromatic hydrocarbons.[46] In addition, the hybrid nanogels have a similar absorption peak centered at 280 nm, indicating that the FCNPs have been successfully immobilized into the poly(NIPAM-AAm) nanogels. Fig. 3b shows a comparison of the FT-IR spectra of FCNPs, poly(NIPAM-AAm) nanogels, and poly(NIPAM-AAm)-FCNP hybrid nanogels. A few features should be noted from the comparison. First, the characteristic absorption peaks of the surface -OH and –COOH groups on free FCNPs are presented in the spectrum of the poly(NIPAM-AAm)-FCNP hybrid nanogels, but the corresponding bands shift from 3360 cm^{-1} to 3430 cm^{-1} for –OH groups and from 1705 cm^{-1} to 1717 cm^{-1} for –COOH groups, respectively. Second, the peaks for amide I and amide II in the free poly(NIPAM-AAm) nanogels are presented in the spectrum of the poly(NIPAM-AAm)-FCNP hybrid nanogels, but the bands shift from 1528 cm^{-1} to 1563 cm^{-1} for amide I and from 1639 cm^{-1} to 1647 cm^{-1} for amide II, respectively. These peak shifts indicate that the surface –OH and –COOH groups on the FCNPs and the amide groups on the poly(NIPAM-AAm) network chains have strong hydrogen bonding interactions in the poly(NIPAM-AAm)-FCNP hybrid nanogels. These results confirm that our strategy, using precipitation copolymerization of NIPAM monomers with the hydrogen-bonding complexes of surface functionalized FCNPs with AAm monomers, is feasible to embed the FCNPs into the poly(NIPAM-AAm) nanogel network. Such designed poly(NIPAM-AAm)-FCNP hybrid nanogels should have very stable optical property because the FCNPs are immobilized in the polymer network via hydrogen bonding interactions.

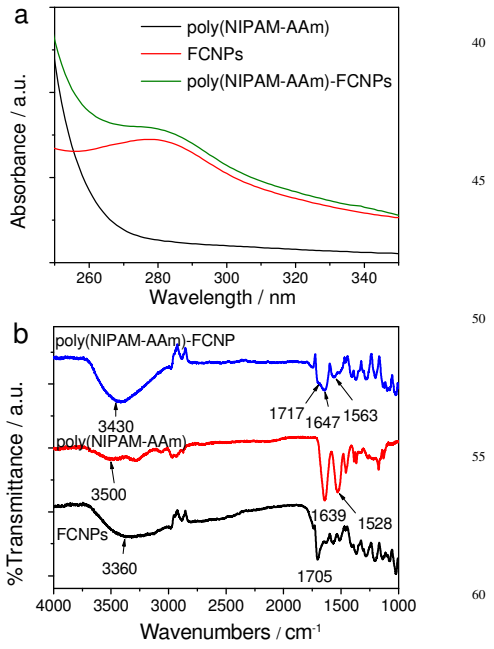

Fig. 3. (a) UV-Vis and (b) FT-IR spectra of the FCNPs, the poly(NIPAM-AAm) nanogels, and the poly(NIPAM-AAm)-FCNP hybrid nanogels, respectively.

To further explore the optical properties of the poly(NIPAM-AAm)-FCNP hybrid nanogels, a detailed PL study was carried out under different excitation wavelengths. Fig. 4a shows typical PL spectra of the FCNPs and poly(NIPAM-AAm)-FCNP hybrid nanogels dispersed in PBS of pH = 7.40, excited at 280 nm and room temperature, respectively. A comparison of the PL spectra of the FCNPs and hybrid nanogels reveals that the emissions at 380 nm of the hybrid nanogels are associated with the embedded FCNPs, which may result from a distribution of the surface energy traps of the carbon nanocrystals (or carbon dots).[47] Fig. 4b shows the PL spectra of the hybrid nanogels excited by longer wavelength light (from 500 to 720 nm) with the up-conversion emissions peaks located in the range from 380 to 540 nm. The upconverted PL property of the hybrid nanogels should be attributed to the multiphoton active process of the FCNPs embedded in the nanogels.[45] These intrinsic PL properties of the hybrid nanogels are very attractive for many biomedical applications.

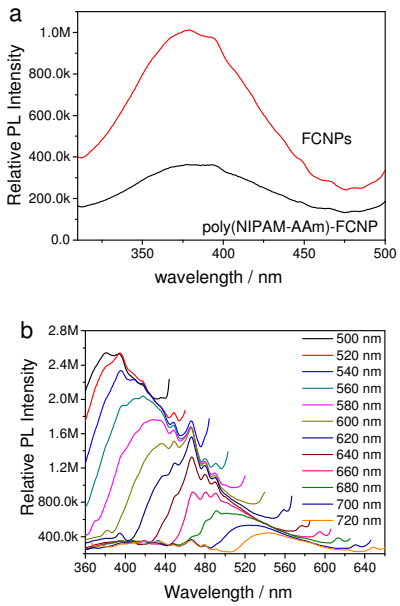

Fig. 4. (a) Typical PL profiles of the FCNPs and poly(NIPAM-AAm)-FCNP hybrid nanogels obtained at λ_{ex} = 280 nm; (b) Upconverted PL spectra of the hybrid nanogels under different excitation wavelengths.

3.2. Temperature-induced volume phase transition of the hybrid nanogels

Fig. 5a shows the temperature-induced volume phase transitions of the poly(NIPAM-AAm) nanogels and poly(NIPAM-AAm)-FCNP hybrid nanogels dispersed in PBS of pH = 7.40, in terms of the change of hydrodynamic diameter (D_h). The increase in temperature induces a gradual shrink of the polymer gel networks. The broad volume phase transition temperature range from 32 to 42 ℃ of the poly(NIPAM-AAm) nanogels is consistant with the previously reported one in the copolymer nanogels with a similar NIPAM/AAm composition ratio.[48] Compared to the free poly(NIPAM-AAm) nanogels synthesized under the same feedings (except no FCNPs) and conditions, the poly(NIPAM-AAm)-FCNP hybrid nanogels demonstrate a similar volume phase transition temperature range, but exhibit a larger size in the whole studied temperature range. The larger size

of the hybrid nanogels than the copolymer template nanogels further support that the FCNPs have been successfully embedded into the poly(NIPAM-AAm) gel networks. The resultant hybrid nanogels demonstrate a very narrow size distribution regardless of their swelling or shrinking states, as shown in Fig. 5b. The thermo-sensitive volume phase transition of such nearly monodispersed hybrid nanogels should provide a temperature-regulated drug releasing behavior when used as drug carriers.

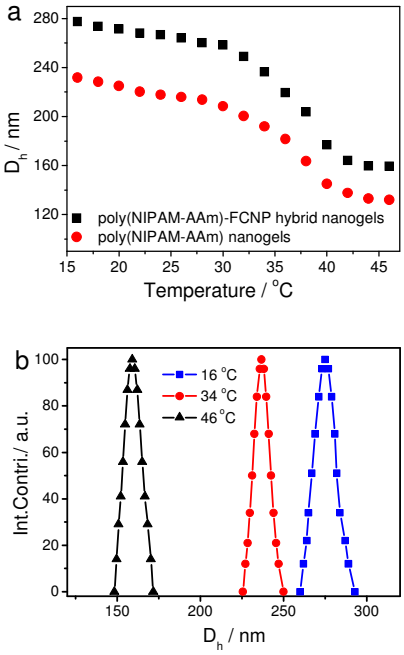

Fig. 5. (a) Temperature dependence of the average D_h values of the nanogels and hybrid nanogels in PBS of pH = 7.40 obtained at a scattering angle θ = 60º. (b) Size distributions of the hybrid nanogels at different temperatures.

3.3. Temperature-sensitive PL property of the hybrid nanogels

Fig. 6a shows the temperature dependent PL spectra of the poly(NIPAM-AAm)-FCNP hybrid nanogels. Interestingly, the temperature-induced shrinking of the poly(NIPAM-AAm) nanogels could significantly enhance the PL intensity emitted from the FCNPs immobilized in the hybrid nanogels. In order to correlate the temperature-induced volume phase transitions and PL intensity enhancement of the poly(NIPAM-AAm)-FCNP hybrid nanogels, the PL intensity of the hybrid nanogels emitted at 380 nm under different temperatures was plotted, as shown in Fig. 6b. The comparison of Fig. 5a with Fig. 6b indicates that a conspicuous increase in the fluorescence intensity of the hybrid nanogels occurred at nearly the same temperature range as that of the gradual decrease in the size of the hybrid nanogels, which indicates that the PL enhancement of the embedded FCNPs is caused by the temperature-induced shrinking of the template polymer nanogels.

Two factors should be responsible for the temperature-sensitive PL enhancement of the hybrid nanogels. One is the increase of the local refractive index surrounding the FCNPs. The local optical electric field surrounding the embedded FCNPs can be tuned by an increase in the refractive index of the poly(NIPAM-AAm) gel networks due to their shrinkage, which leads to an increase in the Rayleigh scattering due to an increased refractive index contrast of the condensed polymer networks to the solvent.[49] On the other hand, the PL enhancement induced by the shrinkage of nanogels may result from the different nonradiative energy loss paths, which is related to the reduction of the number of surface defects. According to the previous reports, the nonradiative energy loss paths are highly dependent on the environmental nature surrounding the FCNPs.[50] At low temperatures, the polymer network chains will tend to expand in water. However, the hydrogen bonding between the polymer chains and the FCNPs hinders the expansion of nanogels to highly swollen states, creating an elastic tension in the bonds at the polymer/FCNP interface, thus producing surface states that could quench the PL. This phenomenon of FCNPs is similar to the temperature-induced PL quenching of colloidal quantum dots (QDs) dispersed in water, where the freezing of dispersion medium propagates the strain to the surface of the QDs, leading to surface quenching states.[51] In contrast, when the temperature increases, the nanogels will be in shrunk states, which decreases the elastic tension and consequently reduce the number of surface trap states acting as emission quenching centers, thus the PL intensity increases. More importantly, a linear correlation between the PL intensity and temperature can be established across the temperature range of 20-42 ºC (inset of Fig. 6b), which is essential for the hybrid nanogels to serve as optical temperature sensor. Furthermore, the temperature-induced PL change of the hybrid nanogels is fully reversible. Fig. 6c shows the PL intensity change of the poly(NIPAM-AAm)-FCNP hybrid nanogels upon ten cycles of heating and cooling processes. The PL spectra were fully reproducible after the repeated heating and cooling due to the reversible thermo-responsive volume phase transition of the poly(NIPAM-AAm) nanogels, which also indicates that the fluorescent FCNPs have been stably immobilized in the nanogel networks. The reversible optical property change is critical for the hybrid nanogels to serve as a sensor and image label agent.

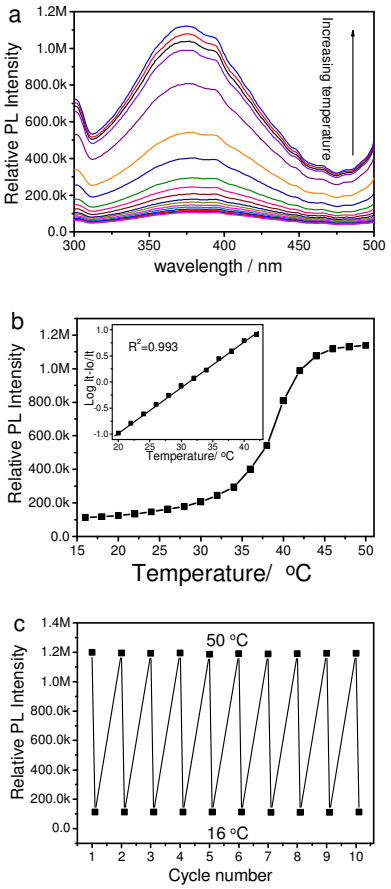

Fig. 6. (a) Typical PL profiles of the hybrid nanogels under different temperatures, taken at 2.0 °C intervals from bottom to

top. (b) Temperature-dependent PL intensity of the hybrid nanogels. (c) Reversible PL intensity change of the hybrid nanogels after ten cycles of repeated heating (50.0 ^{o} C) and cooling (16.0 ^{o} C). All measurements were made in PBS of pH =7.38. Excitation wavelength=280 nm.

3.4. Drug loading and release of the hybrid nanogels

Curcumin, a yellow natural compound possessing excellent pharmaceutical properties including anticancer, antioxidant, antibacterial, antifungal, antiviral, and anti-inflammatory effects,[52-55] was selected as a representative drug for investigating the loading and releasing ability of the hybrid nanogels. Curcumin has low water solubility at pH in acidic or neutral range. At pH in basic range, the compound undergoes rapid hydrolytic degradation. To prevent any significant degradation and realize more efficient loading, the curcumin was loaded into the hybrid nanogels via dropwise adding 4 mL homogeneous solution of 1 mg/mL curcumin in anhydrous ethanol into 5 mL of aqueous dispersion of hybrid nanogels at pH=4.0 placed in an ice water bath,[52,53,56] where the hybrid nanogel is in highly swollen state. Fig. 7a-c shows a comparison of curcumin dispersions after the addition of 4 mL same curcumin ethanol solution into 5 mL of (a) water, (b) poly(NIPAM-AAm) nanogel dispersion, and (c) poly(NIPAM-AAm)-FCNP hybrid nanogel dispersion, respectively, with pH adjusted at 4.0 in all cases. It is very clear that majority of curcumin is undissolved in (a) with macroscopic solid curcumin appearing on the wall and in the bottom of vial, leaving the solution clear with very light yellow color. The presence of poly(NIPAM-AAm) nanogel in the medium increases the overall curcumin solubility due to the complexation interactions of the polymer network chains with the curcumin molecules, resulting in a more homogeneous yellow color of the curcumin dispersion in (b). This result indicates that the poly(NIPAM-AAm) nanogels can carry certain amount of hydrophobic curcumin drug. However, there was still small amount of visible solid curcumin sample appearing in the bottom and wall of vial. In contrast, the aqueous dispersion of the curcumin-loaded poly(NIPAM-AAm)-FCNP hybrid nanogels in (c) is a homogeneously dispersed formulation with its hue derived from the natural color of curcumin. No solid curcumin powder or flakes were visible by naked eyes in the bottom of vial (c), which indicates that the poly(NIPAM-AAm)-FCNP hybrid nanogels can carry more hydrophobic curcumin molecules compared to the free poly(NIPAM-AAm) nanogels. The quantitative analysis determined that the curcumin loading content of the poly(NIPAM-AAm)-FCNP hybrid nanogels and the free poly(NIPAM-AAm) nanogels are 60 and 32 mg/g, respectively, which confirms that the hybrid nanogels have a higher loading capacity for hydrophobic curcumin drug than the free polymer nanogels. This increased curcumin loading capacity of the hybrid nanogels might be attributed to the conjugated aromatic carbon structures of the FCNPs embedded in the gel network, which can associate with curcumin molecules more strongly.

Having demonstrated the curcumin loading ability of the hybrid nanogels, the release experiment of curcumin-loaded hybrid nanogels was carried out. The half-life time for the hydrolytic degradation of curcumin in aqueous solution containing 10% organic solvent has previously been determined to be 4.2×10^{3} h, 15 h and 3.5×10^{-2} h at pH = 6, 7, and 8, respectively.[56] To avoid the evident degradation of curcumin from the long time exposure in water, the in vitro release test was made in a PBS of pH = 6.15. Fig. 7d shows the release kinetics of curcumin from the hybrid nanogels at different temperatures. The increase in temperature could significantly speed up the release of curcumin from the hybrid nanogels. For example, only 21.2% curcumin was released from the hybrid nanogels at 22 ^{o}C after 60 h. In contrast, the amount of curcumin released from the hybrid nanogels reached 36.3%, 48.4%, and 68.2% at temperatures of 37 ^{o}C, 39 ^{o}C, and 41 ^{o}C, respectively, after the same releasing time period of 60 h. The observed temperature dependency of curcumin release should be explained as follows. The increase in temperature could weaken the π-π interactions between the curcumin molecules and the FCNPs, thus increase the mobility of the curcumin molecules. On the other hand, the poly(NIPAM-AAm) polymer becomes more hydrophobic upon heating, thus can hold the drug more tightly. However, the shrunk polymer networks at the elevated temperatures have no enough space to hold all the drug molecules initially loaded. Some drug molecules have to be squashed out of the gel network due to the reduced mesh size. As shown in Figure 5a, the higher the temperature, the smaller the size (or mesh size) of the gel network, but the nanogel network has not reached the minimum collapsing degree even at 41 °C. Correspondingly, more drug molecules have to be squashed out (or released) at a higher temperature in the experimental temperature range of 22-41 °C. At a fixed temperature, the drug release kinetics experience a fast release at initial releasing stage, then slow down, and finally reaching equilibrium with no drugs being further released. Although the shrinkage kinetics of the nanogel particles occurs quite fast, the drug molecules still need time to travel through the shrunk nanogel network. For those drug molecules located near the surface of the gel particles, they can come out from the gel particles easily. That explains why a fast releasing rate was observed at initial stage. However, for those drug molecules located in the center area of the gel particles, they need much long time to travel through the partially shrunk gel network (relatively dense chains), because the release of these drug molecules are not a simple diffusion process due to their strong interactions with the relatively hydrophobic and dense polymer chain networks. The thermo-triggerable curcumin release rate from the hybrid nanogels is important to regulate the drug dose in response to the temperature variation in the pathological microenvironments. In addition, the FCNPs demonstrate an efficient photothermal conversion ability in the NIR wavelength range (Fig. S2), which produces an orthogonal way to trigger the curcumin release from the hybrid nanogels using external NIR irradiation. Fig. 7e shows the release kinetics of curcumin from the hybrid nanogels immersed in a buffer solution irradiated by 1.5 W/cm^{2} NIR light for 5 min at the cumulative time point of 0, 10, 36 and 60 h, respectively. An initial exposure (0 h) to the NIR light for 5 min led to a burst curcumin release. The subsequent exposures to the NIR light for 5 min at different releasing stages also remarkably speed up the drug release. Such a significant increase in release rate within a brief period is undoubtfully attributed to the local heat produced by the efficient photothermal conversion of FCNPs (Fig. S2). When the NIR light was turned off, heating immediately ceased and the drop in temperature brought the drug release back to its regular rates.

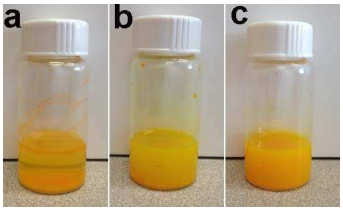

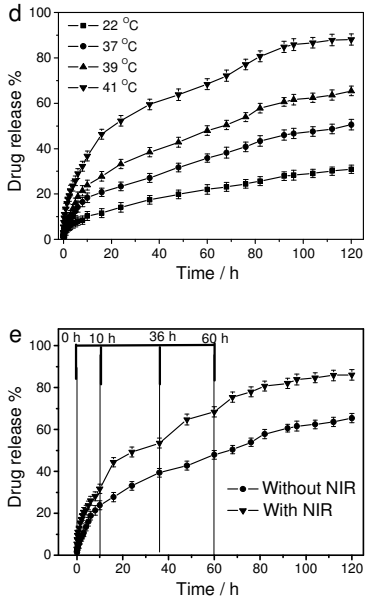

Fig. 7. The photographs of curcumin dispersions in ethanol/water mixture with a same composition, but containing (a) no nanogels, (b) poly(NIPAM-AAm) nanogels, and (c) poly(NIPAM-AAm)-FCNP hybrid nanogels, respectively. Releasing profiles of curcumin from the hybrid nanogels (d) at different temperatures, and (e) at a constant temperature of 37 °C, irradiated with and without 1.5 W/cm^2 NIR for 5 min at cumulative time of 0, 10, 36, and 60 h, respectively.

3.5 Tumor cell internalization of the hybrid nanogels

The emitted fluorescence from the FCNPs immobilized in the hybrid nanogels is very stable. As shown in Fig. S3, the fluorescence spectra of the poly(NIPAM-AAm)-FCNP hybrid nanogels remain nearly no change. The PL intensity at 380 nm only decreases by 1.9 % after a continuous exposure to the excitation light for 2 h in a fluorospectrophotometer. These results indicate that the FCNPs embedded in the poly(NIPAM-AAm) nanogel show excellent photostability against light illumination and the hybrid nanogels have high colloidal stability. After demonstrating the strong and stable fluorescence, the poly(NIPAM-AAm)-FCNP hybrid nanogels were further evaluated as a fluorescence-labeling agent for tumor cell imaging application. Fig. 8 shows laser scanning confocal images of mouse melanoma cells B16F10 incubated with the poly(NIPAM-AAm)-FCNP hybrid nanogels under different exposure time to the excitation laser. Under irradiation of a laser with a wavelength of 405 nm, the FCNPs embedded in the nanogels produced a bright fluorescence, which retained nearly the same PL intensity even after 30 min irradiation. No significant autofluorescence was observed under similar conditions. These results suggest that the hybrid nanogels have good photostability for fluorescent bioimaging. The top-to-bottom z-scanning confocal fluorescence images (Fig. S4) of the B16F10 cells incubated with the hybrid nanogels proves that the hybrid nanogels can overcome cellular barriers to enter into the intracellular region. The hybrid nanogels are located in the cytoplasm, but do not appear in the karyons. Furthermore, the upconversion PL property of the hybrid nanogels may find important applications for bioimaging under excitation of NIR light which can penetrate into biological tissues more effectively than visible light. As demonstrated in Figure S5a, the glass cover slip attached with unlabeled B16F10 cells cannot be observed in the dark image under the NIR light excitation (Odyssey CLx infrared imaging system, λ_{ex} = 700 nm and 800 nm), because the unlabeled cells do not emit fluorescence. In contrast, the cover slip attached with the B16F10 cells incubated with our hybrid nanogels can be clearly imaged under the excitation of same NIR light (Figure S5b), benefited from the bright fluorescence emitted from the hybrid nanogels internalized in the cells under the NIR light irradiation.

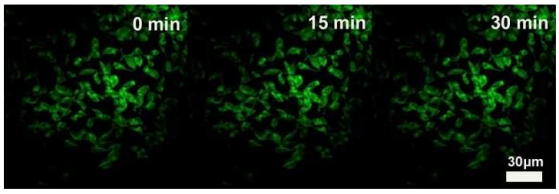

Fig. 8. Laser scanning confocal microscopy images of B16F10 cells incubated with the poly(NIPAM-AAm)-FCNP hybrid nanogels after a continuous exposure to the excitation light with λ_{Ex} = 405 nm.

3.6. In vitro cytotoxicity of the hybrid nanogels

In vitro cytotoxicity of the drug-free and curcumin-loaded hybrid nanogels without and with exposure to 1.5 W/cm^2 NIR light for 5 min was evaluated by means of an MTT test against B16F10 cells. Fig. 9a shows that the drug-free hybrid nanogels have negligible cytotoxicity against B16F10 cells after 24 h incubation in concentrations up to 200 μg/mL. An exposure to the 1.5 W/cm^2 NIR light for 5 min did not change the cell viability of the drug-free hybrid nanogels, indicating that the local heat produced from the photothermal effect of the FCNPs immobilized in the interior of polymer network has minimal effect on cell viability. In contrast, the cell viability decreased by about 25 % after incubated with the curcumin-loaded hybrid nanogels at the same concentrations of nanogels, which demonstrates that the curcumin molecules released from the hybrid nanogels are still active to kill cancer cells. Furthermore, the introduction of 5 min NIR light irradiation can significantly reduce the cell viability during the incubation process with the curcumin-loaded hybrid nanogels. For example, with the 5 min exposure to NIR light, 60% of the B16F10 cancer cells could be killed after being incubated in the curcumin-loaded hybrid nanogels (200 μg/mL) for 24 h. The enhanced cytotoxicity of the curcumin-loaded hybrid nanogels with NIR radiation should be attributed to the synergistic effect of photothermo-/chemo-therapy. Although the local heat produced from the photothermal effect of FCNPs embedded in the interior of nanogels had no much direct damage on cells, the local heat in the hybrid nanogels can speed up the release of loaded curcumin molecules (See Fig. 7e), which have high anti-cancer activity. All above results indicate that the poly(NIPAM-AAm)-FCNP hybrid nanogels can be used as promising drug carriers for combined photothermo/chemo-therapy.

Fig. 9b shows a comparison of the therapeutic efficacies from different treatments. The therapeutic efficacy is calculated by subtracting the cell viability from 100% under the specific treatment. The cell viability treated with the drug-free hybrid nanogels is used as background correction. The photothermal treatments represent that the cells are incubated with the drug-free hybrid nanogels and exposed to 1.5 W/cm^2 NIR light for 5 min. The chemo treatments represent that the cells are incubated with the curcumin-loaded hybrid nanogels, but no exposure to NIR light. The combined photothermal/chemo treatments represent that the cells are incubated with the curcumin-loaded hybrid nanogels plus an exposure to 1.5 W/cm^2 NIR light for 5 min. The additive therapeutic efficacies ($T_{additive}$) was estimated using the relation of $T_{additive} = 100 \times (f_{chemo} - f_{photothermal}) \times 100$, where f is the fraction of surviving cells after each treatment.[57] The therapeutic efficacy of combined photothermal/chemo treatments with the

curcumin-loaded hybrid nanogels was significantly higher than the additive therapeutic efficacy of chemo- and photothermal therapy alone. When *t*-test is used to compare the therapeutic efficacies of the combined photothermal/chemo treatments with the corresponding $T_{additive}$ values, all *p*-values are lower than 0.01, indicating a significant difference. Clearly, the poly(NIPAM-AAm)-FCNP hybrid nanogels as drug carriers demonstrate a highly synergistic effect for combined chemo-photothermal treatments.

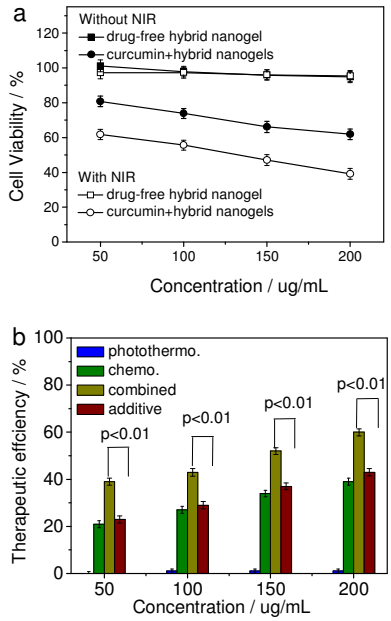

Fig. 9. (a) In vitro cytotoxicity of drug-free and curcumin-loaded poly(NIPAM-AAm)-FCNP hybrid nanogels without and with exposure to 1.5 W/cm^2 NIR light for 5 min, respectively; (b) Comparison of the therapeutic efficacies of the poly(NIPAM-AAm)-FCNP hybrid nanogels as a curcumin carrier for photothermal, chemo, and combined photothermal/chemo treatments.

4. Conclusions

In summary, multifunctional water-dispersible poly(NIPAM-AAm)-FCNP hybrid nanogels can be successfully synthesized through the precipitation copolymerization of NIPAM monomers with the FCNP-complexed AAm monomers. While the poly(NIPAM-AAm) nanogel provides the hybrid nanogels with high colloidal stability and thermo-responsive property, the immobilized FCNPs in the interior of gel network provide the hybrid nanogels with bright, stable, and upconversion PL properties and photothermal conversion ability of NIR light. The resultant hybrid nanogels can overcome cellular barriers to enter the intracellular region and light up the B16F10 cells under a laser excitation. The reversible thermo-sensitive volume phase transition property of the poly(NIPAM-AAm) gel network can modify the physicochemical environment of the embedded FCNPs to manipulate the fluorescence intensity for optical sensor of environmental temperatures. Furthermore, the hybrid nanogel provides a high loading capacity for a highly hydrophobic anticancer drug of curcumin. The drug release rate can be efficiently controlled by changing the temperature of local environmental media or the exogenous irradiation with NIR light. While the drug-free hybrid nanogels are nontoxic to cells, the curcumin-loaded hybrid nanogels exhibit potent cytotoxicity against B16F10 cells. The therapeutic efficacy can be further significantly improved with an orthogonal exogenous NIR irradiation treatment benefited from the photothermal conversion ability of the FCNPs. The demonstrated multifunctional hybrid nanogels with excellent optical properties from the FCNPs and unique properties from the responsive nanogels provide a new idea for the design and fabrication of novel biomaterials and nanomaterials.

Acknowledgements

We gratefully acknowledge the financial support from American Diabetes Association (Basic Science Award 1-12-BS-243) and the PSC-CUNY Research Award (66076-00 44). We thanks a lot for the help from Sumit Mukherjee about the NIR scanner imaging.

Notes and references

[a] *Department of Chemistry, The College of Staten Island, and The Graduate Center, The City University of New York, Staten Island, NY 10314 USA. E-mail address: shuiqin.zhou@csi.cuny.edu; Tel.: +1 718 982 3897; Fax: +1 718 982 3910. A*

[b] *Department of Chemistry and Biochemistry, Hunter College, The City University of New York, New York, NY 10065, USA*

† Electronic Supplementary Information (ESI) available: Figure S1- Figure S5. See DOI: 10.1039/b000000x/

References

1 A. Döring, W. Birnbaum and D. Kuckling, *Chem. Soc. Rev.,* 2013, **42**, 7391.
2 M. Motornov, Y. Roiter, I. Tokarev and S. Minko, *Prog. Polym. Sci.,* 2010, **35**, 174.
3 W. Wu and S. Zhou, *Nano Reviews,* 2010, **1**, 5730.
4 B. Balakrishnan and R. Banerjee, *Chem. Rev.,* 2011, **111**, 4453.
5 H. Park and K. Park, *Pharm. Res.,* 1996, **13**, 1770.
6 W. Wu, T. Zhou, A. Berliner, P. Banerjee and S. Zhou, *Chem. Mater.,* 2010, **22**, 1966.
7 W. Wu, J. Shen, P. Banerjee and S. Zhou, *Adv. Funct. Mater.,* 2011, **21**, 2830.
8 R. Liu, X. Zhao, T. Wu and P. Feng, *J. Am. Chem. Soc.,* 2008, **130**, 14418.
9 P. D. Thornton and A. Heise, *J. Am. Chem. Soc.,* 2010, **132** , 2024.
10 Y. Zhao, B. G. Trewyn, I. I. Slowing and V. S. Y. Lin, *J. Am. Chem. Soc.,* 2009, **131**, 8398.
11 Xiong, M.; Li, Y.; Bao, Y.; Yang, X.; Hu, B.; Wang, J. *Adv. Mater.,* **2012**, *24*, 6175.
12 W. Wu, N. Mitra, E. C. Y. Yan and S. Zhou, *ACS Nano,* 2010, **4**, 4831.
13 S. M. Lee, H. Park and K. H. Yoo, *Adv. Mater.,* 2010, **22**, 4049.
14 Y. T. Chang, P. Y. Liao, H. S. Sheu, Y. J.Tseng, F. Y.Cheng and C. S. Yeh, *Adv. Mater.,* 2012, **24**, 3309.
15 Y. Zhu and M. Fujiwara, *Angew. Chem., Int. Ed.,* 2007, **46**, 2241.
16 T. D. Nguyen, K. C. F. Leung, M. Liong, Y. Liu, J. F. Stoddart and J. I. Zink, *Adv. Funct. Mater.,* 2007, **17**, 2101.
17 E. Aznar, R. Casasus, B. Garcia-Acosta, M. D. Macros, R. Martinez-Manez, F. Sancenon, J. Soto and P. Amoros, *Adv. Mater.,* 2007, **19**, 2228.
18 M. Ferrari and V. Quaresima, *Neuroimage,* 2012, **63**, 921.
19 F. F. Jöbsisvander-Vleit, *J. Biomed. Opt.,* 1999, **4**, 392.
20 J. Nam, N. Won, H. Jin, H. Chung and S. Kim, *J. Am. Chem. Soc.,* 2009, **131**, 13639.
21 S. S. Agasti, A. Chompoosor, C. C. You, P. Ghosh, C. K. Kim and V. M. Rotello, *J. Am. Chem. Soc.,* 2009, **131**, 5728.
22 W. Wu, J. Shen, P. Banerjee and S. Zhou, *Biomaterials,* 2011, **32**, 598.
23 R. Chen, X. Zheng, H. Qian, X. Wang, J. Wang and X. Jiang, *Biomater. Sci.,* 2013, **1**, 285.
24 M. S. Yavuz, Y. Cheng, J. Chen, C. M. Cobley, Q. Zhang, M. Rycenga, J. Xie, C. Kim, K. H. Song, A. G. Schwartz, L. V. Wang and Y. Xia, *Nat. Mater.,* 2009, **8**, 935.
25 H. Wang, J. Shen, Y. Y. Li, Z. Wei, G. Cao, Z. Gai, K. Hong, P. Banerjee and S. Zhou, *ACS Appl. Mater. Interfaces,* 2013, **5**, 9446.

26 J. Jiang, H. Gu, H. Shao, E. Devlin, G. C. Papaefthymiou and J. Y. Ying, *Adv. Mater.,* 2008, **20**, 4403.
27 H. Wang, J. Shen, G. Cao, Z. Gai, K. Hong, P. R. Debata, P. Banerjee and S. Zhou, *J. Mater. Chem. B,* 2013, **1**, 6225.
28 V. I. Shubayev, T. R. Pisanic II and S. Jin, *Adv. Drug Delivery Rev.,* 2009, **61**, 467.
29 T. R. Pisanic II, J. D. Blackwell, V. I. Shubayev, R. R. Finones and S. Jin, *Biomaterials,* 2007, **28**, 2572.
30 H. Li, Z. Kang, Y. Liu and S. T. Lee, *J. Mater. Chem.,* 2012, **22**, 24230.
31 X. Wang, L. Cao, S. Yang, F. Lu, M. Meziani, L. Tian, K. W. Sun, M. A. Bloodgood and Y. P. Sun, *Angew. Chem., Int. Ed.,* 2010, **49**, 5310.
32 R. Liu, D. Wu, S. Liu, K. Koynov, W. Knoll and Q. Li, *Angew. Chem., Int. Ed.,* 2009, **48**, 4598.
33 H. Li, X. He, Z. Kang, H. Huang, Y. Liu, J. Liu, S. Lian, C. H. A. Tsang, X. Yang and S.-T. Lee, *Angew.Chem., Int. Ed.,* 2010, **49**, 4430.
34 Y. Pan, S. Neuss, A. Leifert, M. Fischler, F. Wen, U. Simon, G. Schmid, W. Brandau and W. Jahnen-Dechent, *Small,* 2007, **3**, 1941.
35 S. Yang, X. Wang, H. Wang, F. Lu, P. Luo, L. Cao, M. Meziani, J. Liu, Y. Liu, M. Chen, Y. Huang and Y. P. Sun, *J. Phys. Chem. C,* 2009, **113**, 18110.
36 L. Zheng, Y. Chi, Y. Dong, J. Lin and B. Wang, *J. Am. Chem. Soc.,* 2009, **131**, 4564.
37 Y. Fang, S. Guo, D. Li, C. Zhu, W. Ren, S. Dong and E. Wang, *ACS Nano,* 2012, **6**, 400.
38 S. Yang, L. Cao, P. Luo, F. Lu, X. Wang, H. Wang, M. Meziani, Y. Liu, G. Qi and Y. Sun, *J. Am. Chem. Soc.,* 2009, **131**, 11308.
39 S. P. Sherlock and H. Dai, *Nano Res.,* 2011, **4**, 1248.
40 Z. Yang, M. Wang, A. Yong, S. Wong, X. Zhang, H. Tan, A. Chang, X. Li and J. Wang, *Chem. Commun.,* 2011, **47**, 11615.
41 S. N. Baker and G. A. Baker, *Angew Chem., Int. Ed*., 2010, **49**, 6726.
42 A. Zhu, Q. Qu, X. Shao, B. Kong and Y. Tian, *Angew.Chem., Int. Ed.,* 2012, **51**, 7185.
43 H. Wang, J. Shen, Y. Y. Li, Z. Wei, G. Cao, Z. Gai, K. Hong, P. Banerjee and S. Zhou, *Biomater. Sci.,* 2014, DOI:10.1039/C3BM60297D
44 J. Shen, Y. Zhu, X. Yang and C. Li, *Chem. Commun.,* 2012, **48**, 3686.
45 H. Li, X. He, Y. Liu, H. Huang, S. Lian, S. T. Lee and Z. H. Kang, *Carbon,* 2011, **49**, 605.
46 S. A. Chitrea, G. A. Lobo, S. M. Rathod, R. B. Smith, R. Leslie, C. Livingstone and J. Davis, *J. Chromatogr. B,* 2008, **864**, 173.
47 F. Wang, S. P. Pang, L. Wang, Q. Li, M. Kreiter and C. Y. Liu, *Chem. Mater.,* 2010, **22**, 4528.
48 J. Shen, T. Ye, A. Chang, W. Wu and S. Zhou, *Soft Matter*., 2012, **8**, 12034.
49 R. Contreras-Cáceres, A. Sánchez-Iglesias, M. Karg, I. Pastoriza-Santos, J. Pérez-Juste, J. Pacifico, T. Hellweg, A. Fernández-Barbero and L. M. Liz-Marzán, *Adv. Mater.,* 2008, **20**, 1666.
50 X. Wang, L. Cao, F. Lu, M. J. Meziani, H. Li, G. Qi, B. Zhou, B. A. Harruff, F. Kermarrec and Y. P. Sun, *Chem. Commun.,* 2009, **45**, 3773.
51 S. R. Wuister, C. M. Donegá and A. Meijerink, *J. Am. Chem. Soc.,* 2004, **126**, 10397.
52 B. B. Aggarwal and B. Sung, *Trends Pharmacol. Sci.,* 2008, **30**, 85.
53 B. B. Aggarwal, C. Sundaram, N. Malani and H. Ichikawa, *Adv. Exp. Med. Biol.,* 2007, **595**, 1.
54 S. Singh, *Cell,* 2007, **130**, 765.
55 D. H. Alpers, *Curr. Opin. Gastroenterol.,* 2008, **24**, 173.
56 H. H. Tønesen and J. Karlsen, *Z. Lebensm. Unters. Forsch.,* 1985, **180**, 402.
57 G. M. Hahn, J. Braun and I. Har-kedar, *Proc. Natl. Acad. Sci. U. S. A.,* 1975, **72**, 937.